Robotica (2007) volume 25, pp. 501–509. © 2007 Cambridge University Press
doi:10.1017/S0263574707003396 Printed in the United Kingdom

Imitating human acceleration of a gyroscopic device

Andrej Gams*, Leon Žlajpah and Jadran Lenarčič

Robotics Laboratory, Jožef Stefan Institute, Jamova 39, 1000 Ljubljana, Slovenia.

(Received in Final Form: January 18, 2007. First published online: February 26, 2007)

SUMMARY

Spinning up a Power®ball—a hand-held gyroscopic toy or exerciser that exhibits rotor spin-up when applying appropriate torque to its casing—is a fairly easy task for a human but rather complex to perform with a robot. To accomplish the task of spinning up the rotor of the Power®ball with a robot, we measured the motion of a human and identified the conditions an individual uses for a successful spin-up. Several control approaches were applied to the device mainly using feedback information from the velocity counter and force/torque sensor to synchronize the torque exerted by the device and the motion of the robot. Best human imitation was achieved with two modified learning methods with highest rotor speeds in excess of 1480 rad/s, rating among top 100 world Power®ball players.

KEYWORDS: Rhythmic motion; Synchronization; Gyroscopic device; Imitation.

1. Introduction

Often in the rhythmic task imitation, sufficient dexterity of the system and synchronization with a device or a toy are required for a successful completion of the task, such as juggling, drumming, or playing a yo-yo.[1–3] These tasks are considered fairly easy for a human but are usually quite demanding for a robot.[3] Humans learn how to operate the device following some basic instructions, imitating skilled players, and using sensory motors. Similar applies for a robotic system that uses complex sensory system feedback and control strategies based on domain knowledge.

There are different ways to generate the motion of the robot hand for rhythmic tasks.[3,8] One of the approaches is based on a predefined rhythmic motion pattern, which can be either composed of smooth functions or learned from a human demonstration.[3] To achieve the desired results with a predefined motion pattern, an online control algorithm changes motion parameters. For many juggling tasks there exists a stable open-loop control strategy.[8] Another approach is to generate trajectories online, depending on the state of the device.

When considering control strategies, two theoretical approaches can be distinguished in research on human motion imitation and robotics.[9] One is the motor program theory, which is rooted in a control theoretic approach, and has dominated research on motor control. The alternative approach is based on a dynamical systems perspective that applies the mathematical tools and concepts from nonlinear dynamical systems theory.[9] This paper presents imitating a human spinning up a Power®ball rotor to high speeds by using both control strategies with force/torque, rotational velocity, and robot position feedback.

In Section 2, we first present some basic facts about the kinematics and dynamics of the device. In Section 3, we describe the motion of a human when spinning up the rotor of the device and we determine the behavioral parameters. Our experimental setup, the open-loop control (Section 4.1), the closed-loop control based on different controllers (Section 4.2), and the method for learning rhythmic motion (Section 4.3) are presented. The conclusions are given in Section 5.

*Corresponding author. E-mail: andrej.gams@ijs.si

2. Power®Ball

The Power®ball is a spherical hand-held gyroscopic toy or exerciser (http://www.powerballs.com) that exhibits rotor spin-up when appropriate torques to the supporting frame (the casing) are applied. First patented in 1973 in USA as Dynabee,[12] it was later implemented under different names, such as Roller ball[11] or Gyrotwister. It can be used as a toy, a therapeutic device, or an exerciser. The plastic version in our experiments weighs roughly 240 g and is 70 mm in diameter.

To operate the device, one first has to spin the rotor with a pull of a string. Then, humans rotate the wrist synchronous with the device, thus accelerating the rotor. If the hand motion is not well synchronized, the rotor decelerates and unless the synchronization is established again, the device stops regardless of the efforts of the operator.

A detailed mathematical analysis of the kinematics and dynamics of the device has been given in previous work.[10–13] In the next paragraphs, we review the basics of its kinematics.

The device consists of a rotor and a plastic casing with a spherical circular groove or track that constrains the movement of the rotor.[12] The rotor of the device has two degrees of freedom (DOF), as presented in Fig. 1. The first DOF, also referred to as the primary rotation, is the spin around the v_1 axis while the second DOF is the rotation around the secondary axis of rotation v_2. Secondary rotation results in the travel of the rotor axle around the constraining groove.[10–13] Analogous to the phenomena that occur when spinning pegtops, these could be referred to as spin and precession.[10,13]

The constraining groove is slightly wider than the diameter of the rotor axle and allows the axle of the rotor to tilt slightly,

https://doi.org/10.1017/S0263574707003396 Published online by Cambridge University Press

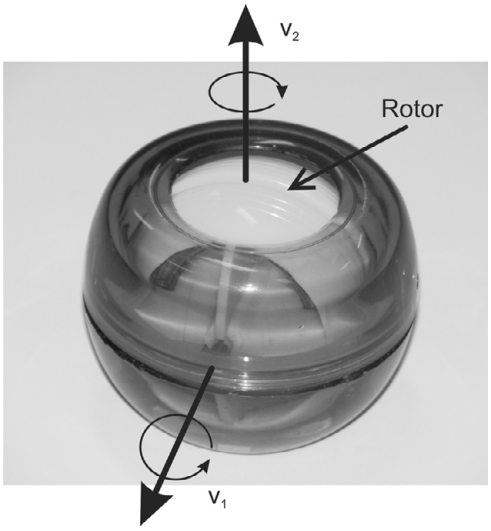


Fig. 1. Power®ball with marked axes of rotor rotation.

as shown in Fig. 2. Consequently, the primary axle (rotating around the v_1 axis) can be in contact with the track on one side on the top and on the other side on the bottom of the axle. When the primary axle is spinning and is in such contact with the track, it can be either rolling or sliding on the track. If it is rolling without sliding on the track at a constant rate, the rotational velocity around the secondary axis is constant, and the ratio between the primary and secondary rotational velocities is governed by

$$\omega_1 = K\omega_2, \tag{1}$$

where ω_1 is the rotational velocity around the primary axis v_1, and ω_2 around the secondary axis v_2. K is determined by the ratio

$$K = \frac{R_2}{R_1}, \tag{2}$$

where R_2 is the distance from the center of rotation of the rotor to the contact point between the rotor and the track, and R_1 is the radius of the primary axle[10] as presented in Fig. 2. For the device in our experiments, K is approximately 31.

The torque applied to the rotor of the device when rolling without sliding is the sum of dissipative torque (as a result of

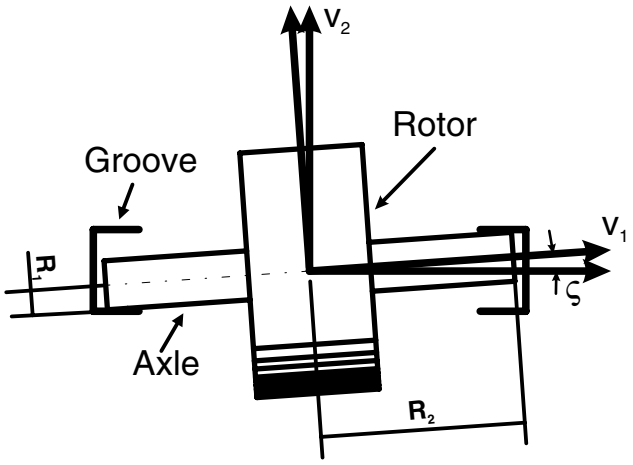


Fig. 2. Constraining groove is slightly wider than the axis of the rotor.

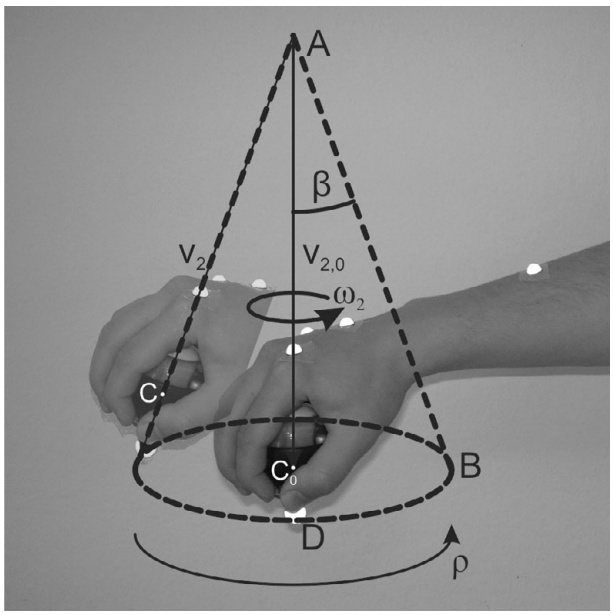


Fig. 3. Positioning of markers for motion capture.

friction and aerodynamic drag) and the torque caused by the track–rotor contact, which constrains the rotor movement. Under the assumption of no dissipation and when ω_1 is constant, the constraining torque equals the torque the holder has to exert.[10] When speeding up, the device tends to tilt more and more, increasing the force between the axle and the track, which in turn increases the torque that increases ω_2. This increases ω_1 according to Eq. (1), thus completing a positive back loop.

3. Human Motion

We measured the human motion when spinning-up the rotor. This was done in different manners, first determining the relevant DOF of the human arm and their movement (Section 3.1), and second, determining the criteria that condition the acceleration or deceleration of the rotor (Section 3.2).

3.1 Motion

The motion of a human arm was measured using the SMART Motion Capture system—a 3D motion capture system consisting of six cameras with infrared stroboscopes and passive reflective markers. The data was acquired at a sampling rate of 60 Hz and with a standard deviation of 0.98 mm. To achieve accurate motion results, the Power®ball was not equipped with additional sensors in the first measurements.

The aim of the measurements was to capture the wrist motion. Hence, the markers were positioned as shown in Fig. 3: three markers were attached to the back of the hand and one marker was attached to the bottom of the device in the line of the v_2 axis. Additional markers were attached to the forearm and upper arm to define the motion of the arm.

Figure 3 shows the hand with the Power®ball in the initial position and during spin-up. The intersection of the v_1 and v_2 axes is marked with C (C_0 in the initial hand position). ρ marks the travel of v_2, which describes the surface of a cone (during spin-up). The angle C_0AB, marked with β, is the

https://doi.org/10.1017/S0263574707003396 Published online by Cambridge University Press

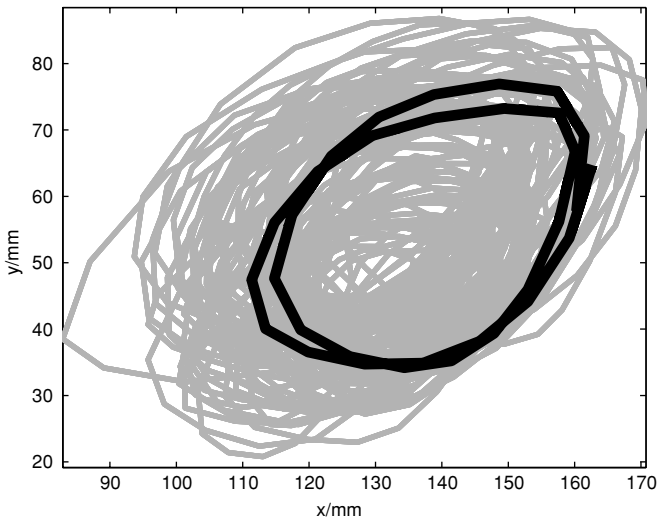


Fig. 4. Recorded track of marker D.

angle between $v_{2,0}$ (initial position) and v_2 (during spin-up). This angle is also referred to as the nutation angle.[10,13] D marks the bottom of the device.

Several spinning-up motions were measured. As expected, the motion was achieved mainly by the wrist, namely, one has to increase the torque to the rotor axle, which cannot be accomplished with translational motion[10,13] and two axes of rotation are sufficient since rotating the device around the v_2 axis has no effect.[13] The two relevant axes of rotation are in the plane of the circular groove of the device and in the initial position of the hand align with the x and y axes of the global coordinate system (CS).

Considering the rotational nature of movement, a circular trace of the marker D (in Fig. 3) was expected. However, Fig. 4 shows elliptic trace of the marker D in the xy plane during rotor acceleration. The trace of two consecutive periods is presented in bold.

There are several reasons why the motion was elliptical but mainly it is because the trajectory of motion is governed by the dexterity limitations and the dynamical properties of the human arm.

Even though the trace of marker D did not turn out to be ideally circular, it does not necessary mean that the v_2 axis of the device does not describe the surface of a cone, as proposed in Fig. 3. Indeed, the measurements of the three markers attached to the back of the hand confirm conical movement of the v_2 axis, as shown in Fig. 5, where approximately one period of motion is presented.

This cone is determined by the angle β (see Fig. 3). The β and the calculated rotor speed ($\omega_{1\,\mathrm{cal}}$) during the spin-up are shown in Fig. 6. To emphasize the approximately constant value of β, the data was filtered with a third-order Butterworth digital filter. As there were no additional sensors on the device, the rotor speed was calculated using Eq. (1), based on the assumption that rolling without sliding was achieved.

From the described measurements it is obvious that humans move the device so that the v_2 axis of the device forms a conical surface in the global CS. Rotations around the two axes in the plane of the constraining groove increase the force

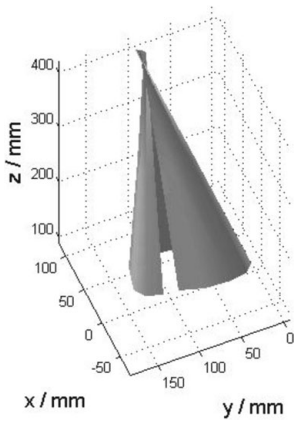


Fig. 5. Conical motion of the v_2 axis.

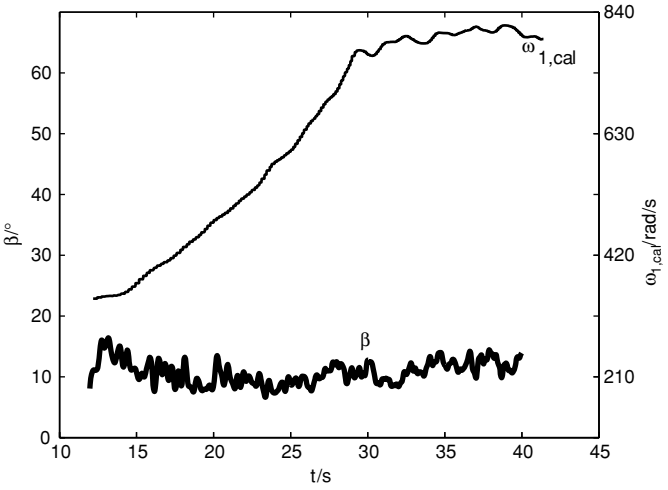


Fig. 6. Filtered β and calculated $\omega_{1\,\mathrm{cal}}$ during rotor acceleration.

of the track–rotor contact, assuming right synchronization with the rotor.

3.2 Movement synchronization

The "catch" of spinning-up a Power®ball is the synchronization of the movement with one of the perceptible quantities. To an operator, it seems as if his hand was constantly leaning on the device. Being famous for the high torques and as suggested from the dynamical analysis,[10] torque seems like a reasonable guess for the synchronization parameter.

To measure the torques we fixed the Power®ball to a JR3 force/torque sensor as shown in Fig. 7. A miniature attitude and heading reference system Xsens Mti was also attached. It is capable of measuring the orientation around all the three axes of rotation in global CS with an accuracy of less that 1° per axis, and was used to measure the rotation of the device. To measure the rotor speed ω_1, the third sensor—a reed relay—was installed into the holder. The rotor speed was determined by counting the pulses caused by a permanent magnet built into the rotor. The added weight and the dimensions of the attached sensors made the operation of the device harder, but we could still achieve spin-up.

https://doi.org/10.1017/S0263574707003396 Published online by Cambridge University Press

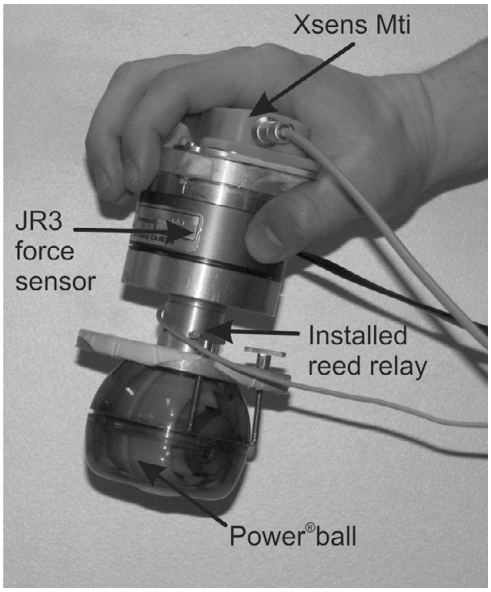


Fig. 7. Setup to measure orientation, rotor speed, and torques.

Figure 8 shows the measured torque and rotation around the relevant axes of rotation as described earlier. At the displayed time interval, rolling without sliding was achieved.

In both plots in Fig. 8 we can see two curves at a phase of $\pi/2$, which is typical for circular motion. The top plot shows the rotations about the x and y axes of the global CS. The signals are marked with β_5 and β_6, which represent motion of the two DOF of the wrist (see Fig. 3). The bottom plot shows the measured torques τ_x and τ_y in the direction of the x and y axes of the sensor. We can define the direction of the torque in the xy plane of the sensor by

$$\phi_\tau = \arctan\left(\frac{\tau_y}{\tau_x}\right). \tag{3}$$

The same can be applied to the orientation of the device by

$$\phi_\beta = \arctan\left(\frac{\dot{\beta}_6}{\dot{\beta}_5}\right), \tag{4}$$

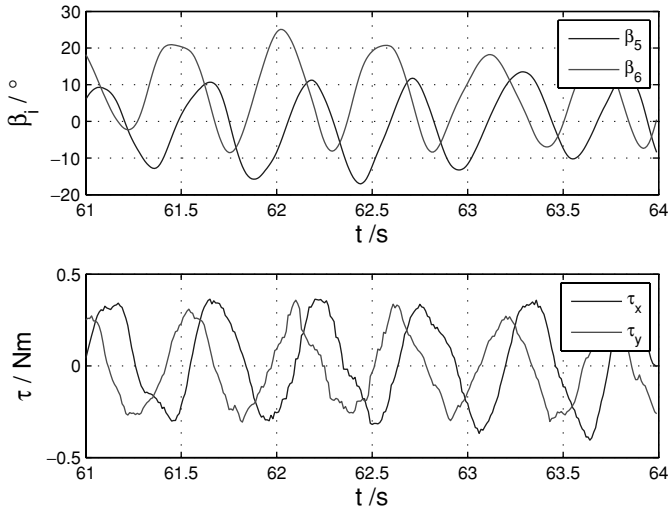


Fig. 8. Measured orientation and torques.

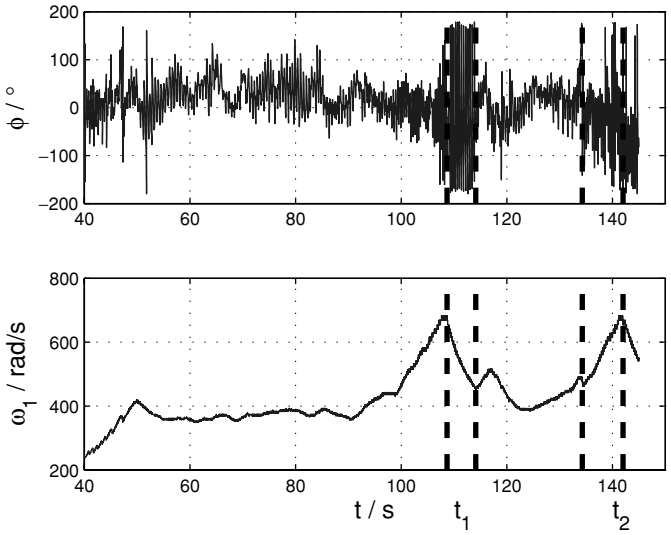


Fig. 9. ϕ and ω_1 for a human operator.

where $\dot{\beta}_5$ and $\dot{\beta}_6$ are rotational velocities around the x and y axes of the global CS. We now introduce a new variable, the "phase" ϕ, defined by

$$\phi = \phi_\tau - \phi_\beta. \tag{5}$$

This phase presented in Fig. 9, defines the relationship between the rotation of the device and the exerted torque.

The phase ϕ shows qualitatively different states of the device (Fig. 9). In the time interval t_1, the rotor is decelerating. Here ϕ changes rapidly between $\pm\ \pi$, which means that the motion of the operator is not synchronized with the device. During most of the presented experiment, the motion is synchronized with the device, therefore the rotational velocity ω_1 is either constant or increasing. When ω_1 is increasing, the phase ϕ decreases, as it can be observed in the time interval t_2.

The ω_1 plot is not fully smooth because of the measuring principle. Namely, by counting the time between rotations of the rotor, the resolution gets lower with higher rotor speeds as one digit accounts for a bigger relative change. To minimize this problem we implemented the measuring algorithm at 5 kHz.

To summarize, the described measurements reveal the necessary motion and the synchronization criteria that a person usually uses for a successful spin-up. The decrease of phase ϕ during the acceleration also indicates a possible strategy for a robotic spin-up, described in the next section.

4. Rotor Spin-up With a Robot

The imitation task of rotor spin-up includes two major challenges. First, the robot motion of the device has to resemble human motion of the device in global CS, and second, the achieved rotor speeds should be comparable to those of an adept operator.

The first task—human arm motion imitation—is only possible if the kinematics of the robot is similar to that of a human arm. Since our robot is not of appropriate structure,

https://doi.org/10.1017/S0263574707003396 Published online by Cambridge University Press

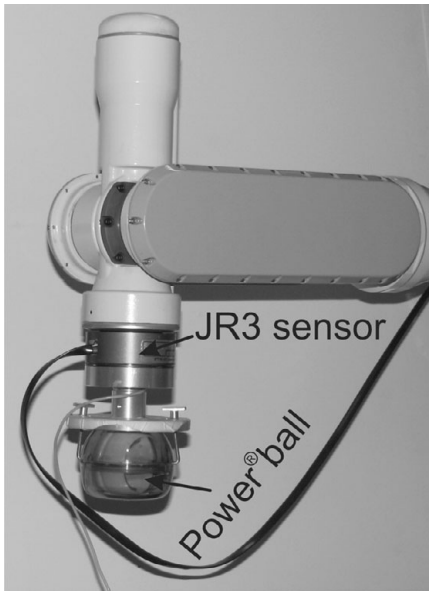


Fig. 10. Experimental setup.

we did not imitate the motion of the human arm, but tried to assure the same motion of the device.

Also the second task seems quite demanding. Until now nobody has reported any spinning of the Power®ball with a robot to the speed of a human operator. Previously published papers on Power®ball mostly dealt with modeling of the device[10,11,13] and did not describe any experimental results. An attempt was mentioned,[13] but no results were presented.

The current world record achieved by a human with the plastic version of Power®ball, like the one in our experiments, is over 1700 rad/s. An average user with some practice usually achieves rotor speeds of about 1000 rad/s.

Our experimental setup consisted of a velocity controlled Mitsubishi PA-10 robot with a mounted six axes JR3 force/torque sensor as shown in Fig. 10. The gripper with the Power®ball was attached to the JR3 sensor and a reed relay was installed into the gripper to measure rotational speed of the rotor, as described in Section 3.2. The control of the robot was realized in the MATLAB/SIMULINK environment. The sampling rate of the controller was 100 Hz.

In our experiment the desired motion was achieved by two wrist axes, i.e., the fifth and sixth DOF of the robot. As explained in the previous sections, this enabled us to imitate the motion of the device.

We tested different control strategies. Table 1 presents seven of the tested control strategies where the robot accelerated the Power®ball, and the human spin-up for comparison. We first approximated the human motion with a sinusoidal signal. Using open-loop control (rows 1 and 2) we showed that the same basic behavioral parameters apply to human and robotic motion. To improve the spin-up, we controlled these behavior parameters in different manners as presented in the table. Rows 3 and 4 present results using classical controllers. We first determined the parameters of the PI regulator and then changed them according to the state of the system with a fuzzy regulator. Row 5 presents the results of spin-up that exploit the kinematics of the device as given in Eq. (1). Finally, rows 6 and 7 present the results of two approaches using a statistically learned signal for the motion imitation. In the table the acceleration time is the time interval between the moment of achieving synchronisation, and when the maximal ω_1 is achieved. In column 4, type of the human imitation is presented (from basic, using a sinusoidal signal, to advanced, being learned from demonstration). In the last column, the maximal achieved ω_1 is given.

The experiments are described in more detail in the following subsections.

4.1 Open-loop control

Considering the two sinusoidal movements of the wrist presented in Fig. 8 and the suggested circular pattern,[10] we used two sinusoidal signals at a phase of $\pi/2$. So, the motions of the two DOF of the robot are $q_5 = \sin(2\pi\nu t)$ and $q_6 = \sin(2\pi\nu t + \pi/2)$. Here, ν is the input frequency, and q_5 and q_6 are joint coordinates.

To check the similarity with the human motion, we first compared the exerted torques during constant rotational motion of the robot with those measured during a human trial. The exerted torques with gravity compensation[14] are shown in the top plot of Fig. 11. Data filtered with a third-order Butterworth digital filter, plotted over the same plot,

Table 1. Different approaches to accelerating the rotor with a robot.

Type of Control	Control Parameter	Average Acceleration Time (s)	Human Imitation	Max ω_1 (rad/s)
Open loop B*	/	35	Sinusoidal signal (basic)	470
Open loop C**	/	130	Sinusoidal signal (basic)	>1050
Closed loop PI	ϕ	230	Sinusoidal signal (modest)	810
Closed loop Fuzzy	ϕ	230	Sinusoidal signal (modest)	840
Velocity control	ω_2	105	Sinusoidal signal (modest)	840
Synchronization with learning	ϕ through synchronization	10	Learned from demonstration (advanced)	1000
Synchronization with learning and phase delay	ϕ through synchronization + phase delay	10+13	Learned from demonstration (advanced)	1489
Human operator	ϕ through synchronisation	10–15		~1000*** 1700****

*Constant velocity amplitude, **Constant position amplitude, ***Average user, ****World record.

https://doi.org/10.1017/S0263574707003396 Published online by Cambridge University Press

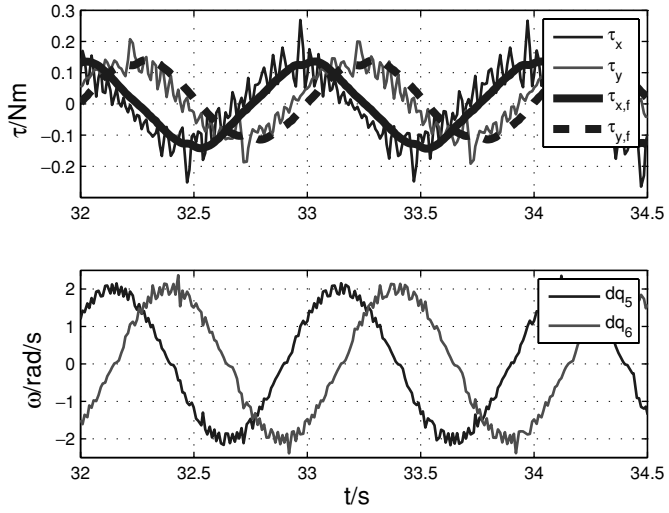


Fig. 11. Measured (τ_x, τ_y) and filtered ($\tau_{x,f}$, $\tau_{y,f}$) torques around the x and y axes of the sensor, and joint velocities of the two DOF.

clearly shows two sinusoidal signals at a phase of $\pi/2$, as observed when measuring human motion. The bottom plot shows the velocity of the two DOF of the robot.

As in Section 3.2 we denote the torque angle ϕ_τ by Eq. (3), but the velocity angle ϕ_q by

$$\phi_q = \arctan\left(\frac{\dot{q}_6}{\dot{q}_5}\right), \tag{6}$$

where $\dot{q}_5$ and $\dot{q}_6$ are robot velocity signals. Again, we introduce the phase ϕ defined as

$$\phi = \phi_\tau - \phi_q, \tag{7}$$

which describes the relation between the torque and the device orientation. As explained in the following, different open-loop control strategies show different behaviors of the phase ϕ.

a) Constant rotational motion

For this and all other experiments, we first started the rotor rotation with a pull of a string and started the robot's motion, in this case with a frequency $\nu_a = 1$ Hz. The results are shown in Fig. 12. We can see that ω_{1a} stabilizes at just over 190 rad/s and that ϕ also stabilizes at a constant value.

b) Accelerated rotational motion with constant velocity amplitude

To generate accelerated motion we controlled the joint velocities using a chirp signal $\dot{q}_{5d} = a\cos(f(t))$, $\dot{q}_{6d} = a\sin(f(t))$, where $f(t) = \int_0^t 2\pi\nu_b(t)\,\mathrm{dt}$, and a is the amplitude of the desired rotational velocity. The frequency of the robot's rotational motion ν_b was empirically set as $\nu_b = (1\ \mathrm{s}^{-1} + 0.03\ \mathrm{s}^{-2}t)$. As shown in the top plot of Fig. 13, the rotational velocity ω_{1b} suddenly starts to decrease at $\omega_{1b} \approx 470$ rad/s ($\nu_b \approx 2.49$ Hz). The reason is that the rotor axle starts to slide.

During the acceleration, ϕ_b is slowly decreasing as ω_{1b} is increasing, the torques and velocities are synchronized and the rotor axle is rolling along the track. During the deceleration, large oscillations of ϕ_b are present as torques and velocities are not synchronized. This resembles the measured phase ϕ from the human motion.

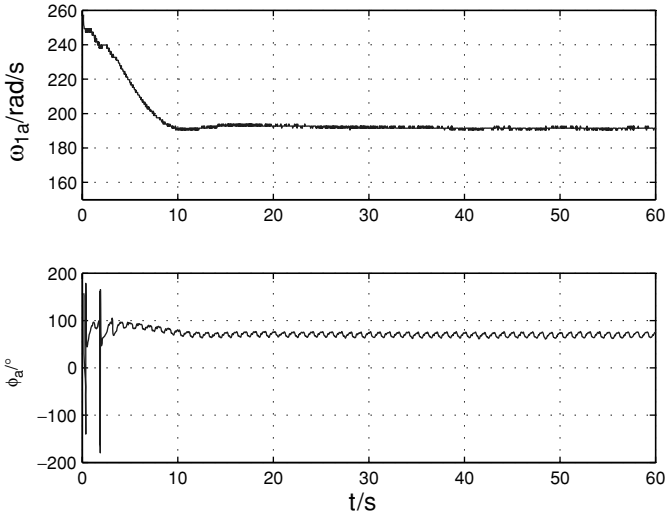


Fig. 12. ω_{1a} and ϕ_a during rotation with constant input frequency.

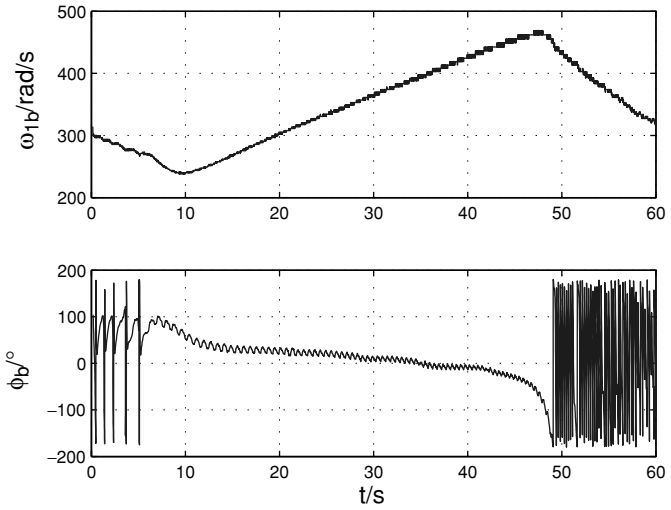


Fig. 13. ω_{1b} and ϕ_b during open-loop acceleration with constant joint velocity amplitude.

c) Accelerated rotational motion with constant position amplitude

The dynamical model[10] assumes a constant nutation angle β (Fig. 3), which is not valid for case b). To achieve constant β, we applied the chirp signal to the joint position with the same acceleration as in case b. The results are presented in Fig. 14.

We can see that the phase did not change with higher speed and that rotor speeds above 1000 rad/s were achieved. Even though the measured velocity (with it also the position) and the torque are synchronized, and the basic movement is similar to the humans', the open-loop control cannot fully resemble how the humans control the motion.

4.2 Closed-loop control

4.2.1 Control with PI controller. As shown in Fig. 13, decreasing ϕ increases the rotational velocity when the

https://doi.org/10.1017/S0263574707003396 Published online by Cambridge University Press

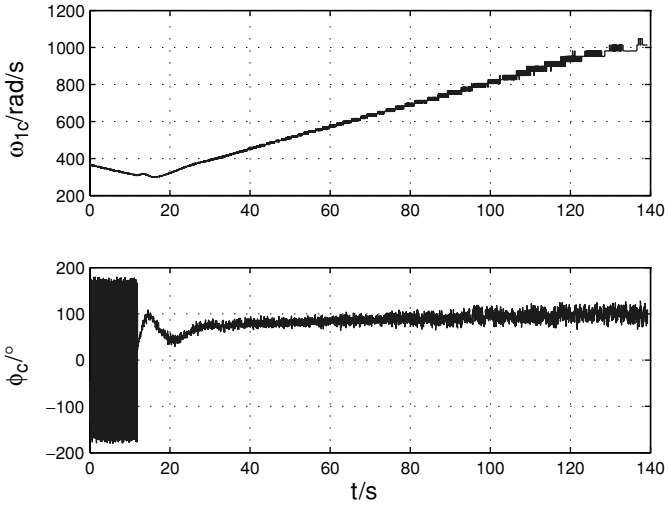


Fig. 14. ω_{1c} and ϕ_c during open-loop acceleration with constant position amplitude.

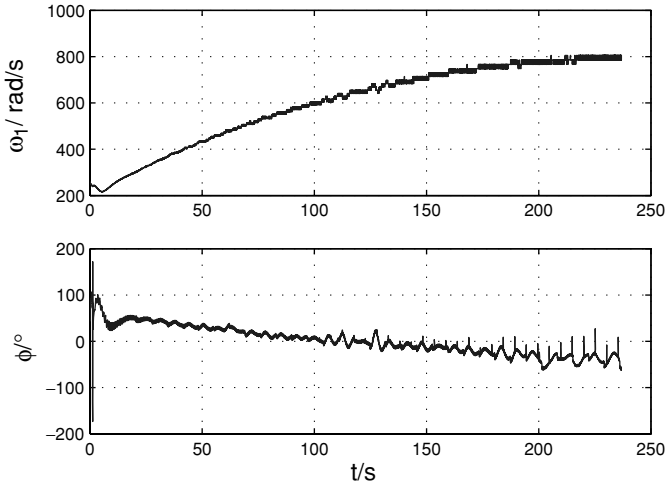


Fig. 15. Closed-loop control with PI controller.

velocity amplitude is constant. To consider this in the control strategy, a predefined value of ϕ_d was selected as the desired value. The acceleration of ν was then controlled so that the synchronization with the device was not lost. We used a PI controller:

$$\nu = \nu_0 + k_p e_\phi + \int k_i e_\phi \, dt, \tag{8}$$

where e_ϕ is given by

$$e_\phi = \phi_d - \phi, \tag{9}$$

and k_p and k_i are the proportional and the integral gain, respectively. Figure 15 shows the results.

The acceleration is slow and decreases over time because the PI controller implies a lower change of ν for lower e_ϕ. Higher acceleration at low rotor speeds is undesired since system stability margin is smaller for lower ω_1.[10] Furthermore, at higher rotor speeds ϕ fluctuates, which results in constant rotor speed. Hence, the PI controller enabled us to achieve maximum rotor speeds around 810 rad/s.

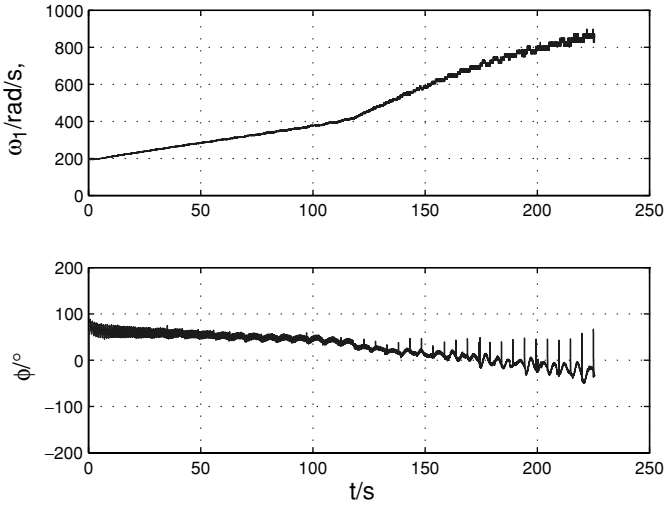


Fig. 16. Closed-loop control with fuzzy controller.

4.2.2 Fuzzy control. To solve the acceleration problem described in 4.2.1, we implemented a fuzzy controller. We again used the PI controller given by Eqs. (8) and (9). However, the proportional gain k_p and the integral gain k_i defined the fuzzy controller and are set according to ϕ and ω_1 as

$$k_p = k'_p + k_{p\omega} \arctan(w_1 - w_c), \tag{10}$$

$$k_i = k'_i + k_{i\omega} \arctan(w_1 - w_c). \tag{11}$$

k'_p and k'_p are calculated by:

$$k'_p = \sum_{j=1}^{3} \mu_j(\phi) k_{p,j}, \tag{12}$$

$$k'_i = \sum_{j=1}^{3} \mu_j(\phi) k_{i,j}. \tag{13}$$

Here, μ are triangular membership functions, $k_{p\omega}$ and $k_{i\omega}$ scale the effect of the ω_1 to the controller output, $\omega_c = 418.88$ rad/s (4000 rpm) is an empirically selected value, and $k_{p,j}$ and $k_{i,j}$, for $j = 1, \ldots, 3$, is the set of empirically selected proportional and integral parameters, respectively. As expected, results in Fig. 16 show a slow initial acceleration and decrease in ϕ, and higher acceleration after achieving $\omega_1 = \omega_c$.

The spikes of ϕ in Fig. 16 are due to too slow acceleration, which causes the axle of the rotor to jump.

4.2.3 Velocity control. In this experiment we controlled the frequency ν to be all the time slightly above ω_2 through

$$\nu = K_1 \omega_1 > \omega_2, \tag{14}$$

where K_1 was empirically set. Figure 17 shows the results of the successful velocity control. However, the acceleration is difficult to achieve, especially at low speeds. Namely, if ω_1 decreases slightly, so does ν, which can lead to deceleration, and the trial fails.

https://doi.org/10.1017/S0263574707003396 Published online by Cambridge University Press

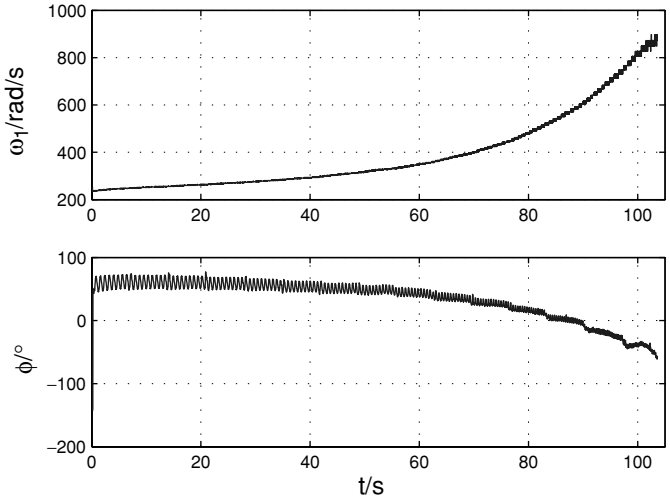


Fig. 17. Rotor acceleration with velocity control.

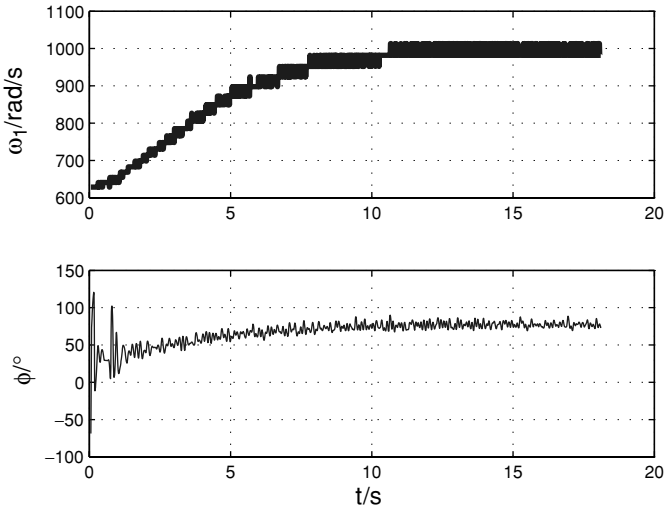


Fig. 18. Motion imitation with learning.

4.3 Synchronizing motion with learning and additionally varying phase

To further improve the human imitation and to achieve higher rotor speeds, we used a well-known imitation technique[1,2,4–7] and modified it to suit the specifics of the device.

4.3.1 Motion synchronization with learning. In their original work[1] Ijspeert et al. used a learning method to imitate rhythmic movements. Starting from a canonical limit cycle oscillator with well-defined stability properties, they modified the attractor landscape of the canonical system by means of a statistical learning method (i.e., regression) to embed arbitrary smooth target patterns.

The canonical nonlinear oscillator has a stable limit cycle behavior characterized by a closed trajectory (circumference) on a phase plane.[1] Instead of using a canonical nonlinear oscillator to create limit cycle behavior; exerted torque by the Power®ball in the *xy* plane of the torque sensor can be used. Based on this limit cycle (as opposite to a nonlinear oscillator limit cycle) we can introduce a control policy[1] of first-order dynamics with a nonlinear function *f*, so that the target trajectory f_t is

$$f_t = \dot{y}_{\text{demo}} - \gamma(y_p - y_{\text{demo}}), \tag{15}$$

where y_{demo} is a demonstrated trajectory, γ is a positive constant, and y_p is a parameter which sets the baseline around which y_{demo} oscillates. The target trajectory f_t, given by a human demonstration, is calculated by

$$f_t = \frac{\sum_{i=1}^{N} \Psi_i w_i^T \tilde{z}}{\sum_{i=1}^{N} \Psi_i} \tag{16}$$

and the Gaussian kernel functions are

$$\Psi_i = e^{(-0.5\, h_i(\varphi - c_i)^2)}. \tag{17}$$

The phase variable $\varphi = \text{atan}\,2\,(M_y, M_x)$ anchors the Gaussian kernel functions and $\tilde{z}$ is the driving signal for Eq. (15). The parameters h_i and c_i determine the location and width of each basis function. The parameters w_i are learned to fit the given demonstration sample trajectory.

Learning the w_i parameters requires solving a nonlinear function approximation. This can be done using incremental locally weighted regression[1,2,4–6] technique in which w_i is updated by

$$w_i^{t+1} = w_i^t + P_i^{t+1} \tilde{z} e_i, \tag{18}$$

where

$$P_i^{t+1} = \frac{1}{\lambda}\left(P_i^t - \frac{P_i^t \tilde{z}\tilde{z}^T P_i^t}{\frac{\lambda}{\Psi_i} + \tilde{z}^T P_i^t \tilde{z}}\right), \quad e_i = f_t - w_i^T \tilde{z}, \tag{19}$$

and λ is the forgetting factor.[1] We can use the same signal to generate the rhythmic drive for multiple DOF[1] and in our case we used it for two DOF.

With the learning algorithm, the robot learns to synchronize the exerted torque from the device with the position reference signal. We know from the previous measurements that during synchronization the torque and the position are proportional: $q_6 \propto \tau_x$, $q_5 \propto -\tau_y$. Figure 18 shows the results.

As we can see, the rotor rapidly accelerates up to 1010 rad/s (∼9600 rpm), and then maintains a constant velocity. The reached velocity depends on all introduced delays, i.e., if we use another filter or bandwidth of the filter, different final velocities are achieved. In the presented case, we used a second-order Butterworth digital filter with the cut-off frequency 10 Hz.

4.3.2 Motion synchronization with learning and a phase delay. To avoid the problem of stalling acceleration, we introduced a phase delay. This approach remains the same as the one described in Section 4.3.1, but with controlled ϕ after ω_1 stabilization. As shown in Fig. 19, after 20 s, when the velocity is clearly constant due to the introduced delays, a linearly increasing phase delay between the measured and learned signal was introduced. This caused the rotor to accelerate further. The phase delay increased to just

https://doi.org/10.1017/S0263574707003396 Published online by Cambridge University Press

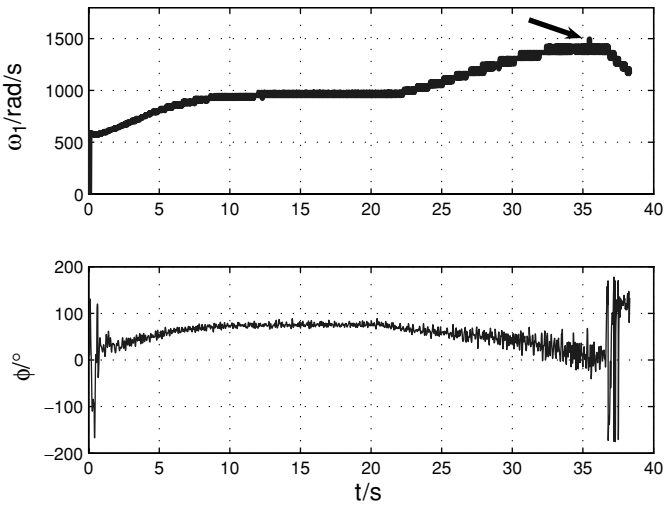


Fig. 19. Motion imitation with learning and additional phase variation.

over 0.4π, when the physical limitations of the robot were reached. The final velocity achieved (marked with an arrow) was 1489 rad/s (14286 rpm).

5. Conclusion

This paper presents different robotic approaches to accelerate the rotor of a Power®ball. One of the goals was also to imitate the human motion when operating the device. We compared different approaches and proposed different methods for learning rhythmic motion.[1]

The rotor acceleration can be achieved in different ways, not necessarily human-like. The comparison showed that the modified learning approach,[1] achieved the best results, and at the same time it was the most human-like. By using one of the perceptual variables—the torque—to attain circumferential limit cycle behavior, we effectively bypassed the need to empirically determine the frequency of the measured periodic signal and thus achieved synchronization. Even so, some delay was introduced by measuring and filtering of the signal. Therefore, the synchronization was not perfect. An additional introduction of a phase delay was another modification of the original learning method that exploits the specifics of the device and enables achieving the desired rotor speed.

The resulting motion was indeed human-like—its trajectory the same to that of a human, it exploited the same parameters for a spin-up, and achieved similar or even better results than an average human operator.

The achieved results were actually even better since the robot had to operate the device with the sensor and gripper attached. With the same load an average human operator could barely achieve 800 rad/s, comparing to the 1489 rad/s achieved by the robot. In the fastest experiments, the robot reached its physical limitation, preventing it from accelerating any further. Even so, the achieved rotor velocity would suffice to place our robot around place 70 on the World Top 100 Power®ball Scoreboard.

References

1. A. J. Ijspeert, J. Nakanishi and S. Schall, "Learning Rhytmic Movements by Demonstration Using Nonlinear Oscillators," *Proceeedings of the 20002 IEEE/RJS International Conference on Intelligent Robots and Systems*, Laussane, Switzerland (2002) pp. 958–963.
2. A. J. Ijspeert, J. Nakanishi and S. Schaal, "Movement Imitation With Nonlinear Dynamical Systems in Humanoid Robots," *Proceedings of the IEEE International Conference on Robotics and Automation*, Washington, DC, USA (2002) pp. 1398–1403.
3. L. Žlajpah, "Robotic yo-yo: modelling and control strategies," *Robotica* **24**(2), 211–220 (2006).
4. A. J. Ijspeert, J. Nakanishi and S. Schaal, "Learning Attractor Landscapes for Learning Motor Primitives," *Proceedings of the Advances in Neural Information Processing Systems 15* (S. Becker, S. Thrun and K. Obermayer, eds.) (2002) pp. 1547–1554.
5. A. J. Ijspeert, J. Nakanishi and S. Schall, "Trajectory Formation for Imitation With Nonlinear Dynamical Systems," *Proceedings of the IEEE/RJS International Conference on Intelligent Robots and Systems* (2001) pp. 752–757.
6. D. Pongas, A. Billard and S. Schaal, "Rapid Synchronization and Accurate Phase-Locking of Rhythmic Motor Primitives," *Proceedings of the IEEE International Conference on Intelligent Robots and Systems*, Edmonton, Canada (2005) pp. 2911–2916.
7. S. Schaal and C. G. Atkeson, "An implementation of memory-based learning," *Control Syst. Mag.* **14**(1), 57–71 (1994).
8. S. Schaal and C. G. Atkeson, "Open Loop Stable Control Strategies for Robot Juggling," *Proceedings of the IEEE Conference on Robotics and Automation*, Atlanta, Georgia (1993) pp. 913–918.
9. S. Schaal, D. Sternad and C. G. Atkeson, "One-handed juggling: a dynamical approach to a rhytmic movement task," *J. Motor Behav.* **28**(2), 165–183 (1996).
10. D. W. Gulick and O. M. O'Reilly, "On the dynamics of the Dynabee," *J. Appl. Mech.* **67**, 321–325 (2000).
11. P. G. Heyda, "Roller ball dynamics revisited," *Am. J. Phys.* **70**(10), 1049–1051 (2002).
12. A. L. Mishler, "Gyroscopic Device," U.S. Patent 3726146 (1973).
13. B. Curk, "Robotiziran Powerball®," *Proceedings of Zbornik ERK 2006 Zvezek B*, Portorož, Slovenija (2006) pp. 167–170.
14. D. Omrčen and B. Nemec, "Measuring knee movement using an industrial robot—gravity compensation for the automatic gripper," *Strojniški vestnik* **48**(2), 87–98 (2002).

https://doi.org/10.1017/S0263574707003396 Published online by Cambridge University Press